Evaporation residue, fission cross sections, and linear momentum transfer for ^{14}N induced reactions from 35*A* to 155*A* MeV

A. A. Sonzogni, A. Elmaani, C. Hyde-Wright, W. Jiang, D. Prindle, and R. Vandenbosch
Nuclear Physics Laboratory, University of Washington, Seattle, Washington 98195

J. Dinius, G. Cron, D. Bowman, C. K. Gelbke, W. Hsi, W. G. Lynch, C. Montoya, G. Peaslee, C. Schwarz, M. B. Tsang, and C. Williams
National Superconducting Cyclotron Laboratory, Michigan State University, East Lansing, Michigan 48824

R. DeSouza, D. Fox, and T. Moore
Indiana University Cyclotron Facility, Indiana University, Bloomington, Indiana 47405
(Received 8 May 1995)

Differential cross sections for evaporation residues and fission fragments for 35*A*, 100*A*, 130*A* and 155*A* MeV ^{14}N on targets ranging from ^{154}Sm to ^{197}Au have been measured. The angle-integrated cross sections are larger than what might be expected. The fission fragment-fission fragment folding angle correlations for 35*A*, 100*A* MeV ^{14}N and 25*A* MeV ^{16}O on similar targets were also measured. The average linear momentum transfer has been deduced from both the fission angle correlation and from the fore-aft asymmetry of the fission angular distributions in the laboratory system. The data are all consistent with a picture where pre-equilibrium particle emission removes an increasing fraction of the orbital angular momentum as the bombarding energy increases. This allows a large range of partial waves to contribute to formation of a composite nucleus with a finite fission barrier.

PACS number(s): 25.70.Jj

I. INTRODUCTION

The mechanisms of an intermediate energy heavy ion reaction are very dependent on the impact parameter of the collision. The largest impact parameters lead to quasielastic reactions, with somewhat smaller impact parameters leading to more deeply inelastic collisions. A wide range of impact parameters leads to complete and incomplete fusion (fusionlike) processes. In the study of reaction mechanisms it is very valuable to have a tag which measures the impact parameter of a particular collision. A variety of tagging techniques have been suggested or applied, depending on the bombarding energy and the impact parameter range of interest [1–3]. γ-ray multiplicities can be used at low energies and small impact parameter, but become nonmonotonic at larger impact parameters as the γ-ray multiplicity starts to drop with increasing impact parameter. Light charged particle (LCP) multiplicities are the most popular tag at intermediate energies, but they are most useful at large impact parameter and for heavy systems. For impact parameters within the fusionlike range the fluctuations in the LCP multiplicity becomes larger than the variation in the mean multiplicity over this range of impact parameters [1]. A similar situation holds for the variation of the mean linear momentum transfer in this impact parameter regime. A new tagging technique for defining different mean impact parameter regions within the fusionlike regime has been proposed and used in a previous study [4]. It is based on the angular momentum dependence of evaporation residue-fission competition in the $A = 160–210$ region. Low impact parameter (and hence low angular momentum) events lead to evaporation residues, and higher impact parameter (higher angular momentum) events lead to fission. Detection of residues or fission fragments in a particular event allows tagging. The mean impact parameter for a particular kind of tag can be adjusted by changing slightly the mass and charge of the target and therefore changing the fissionability of the composite system. In order to know the mean angular momentum for a particular kind of tag it is necessary to know the absolute evaporation residue and fission cross sections for each target at every bombarding energy of interest. This paper reports the results of such measurements. They will be used in the analysis of an experiment which has been performed to study the impact parameter dependence of producing different light charged particles and intermediate mass fragments and to determine the lifetime of hot, well-characterized systems. They are also of importance in the planning of future experiments to measure the sign of the deflection angle at high bombarding energy [5].

In addition to determining the division of the fusionlike cross section between evaporation residues and fission, it is important to also characterize the momentum transfer to the composite system. The probability for complete fusion of projectile and target nucleus becomes vanishingly small for heavy ion collisions in the intermediate energy domain between 20 and 100 MeV per nucleon [6–9]. Pre-equilibrium particle emission results in the final formation of a composite nucleus with fewer nucleons than the sum of the projectile and target nucleons, and with less momentum and excitation energy than would have resulted from complete capture of the projectile. The mean momentum transfer can be determined from the fission fragment-fission fragment folding angle correlation function. It can also be deduced from the fore-aft asymmetry of the fission fragment singles distributions in the laboratory frame. The results of these measurements will be given here.

II. EXPERIMENT

In this paper we report the results of an experiment performed at the National Superconducting Cyclotron Laboratory at Michigan State University using the Miniball array [10]. The K1200 Cyclotron was used to deliver 35*A*, 100*A*, 130*A*, and 155*A* MeV ^{14}N beams on four targets, ^{154}Sm, ^{159}Tb, ^{181}Ta, and ^{197}Au, respectively 0.63, 1.5, 1.2, and 1.5 mg/cm^2 thick. Linear momentum transfer measurements were also made with a 25*A* MeV ^{16}O beam.

The evaporation residue (ER) angular distributions were measured using two different groups of detectors. The first group was placed at the most forward angles (3°–24°) and consisted of 4 Si telescopes. The first element (20–400 μm thick) was thick enough to stop all the ER and fission fragments (FF) and gave us an energy and a time signal. The second element (400–1000 μm thick) was used as a veto detector. The ER and FF were identified through their distinctive signature in a two-dimensional plot of energy versus time of flight.

The second group of detectors consisted of 10 ion chamber (IC) detectors placed at fixed angles from 12.5° to 150°. Each IC consisted of 3 sections, gas, Si, and CsI. The evaporation residues were stopped in the gas detector while the FF could punch through it and reach the Si detector. The CsI was used as a veto. As in the previous case, two-dimensional plots ($E_{\rm gas}$ vs $E_{\rm Si}$) were used to separate the ER from FF.

To measure the fission folding angle we also used the Miniball phoswich detectors to identify the coincident fragment [10–12]. This was achieved by exploiting the fact that the fission fragments deposited almost all of their energy in the first thin plastic element and very little in the second CsI element of the phoswich detector. We also required that these complementary FF be co-planar to the primary fragment detected in one of the IC's. The relative azimuthal angular correlation showed most complementary FF to be within 30° of the fission plane. The background outside the co-planarity region was uniform and estimated to be less than 5%.

Finally, 4 additional Si detectors were placed at a polar angle of 2.75° and azimuthal angles of 0°, 90°, 180°, and 270° and used as monitors.

III. CROSS SECTION AND ANGULAR DISTRIBUTIONS

The ER and FF angular distributions were measured for ^{14}N at 35*A*, 100*A* MeV on ^{154}Sm, ^{159}Tb, ^{197}Au, and ^{14}N at 130*A*, 155*A* MeV on ^{154}Sm, ^{197}Au.

A check was made for ^{14}N at 35*A* MeV on the Sm, Tb, and Au targets to see if the experimental elastic cross section, obtained from the beam current integrator, the target thickness and assuming charge state = 7, was comparable to that predicted by Rutherford scattering. At this energy the ER and FF experimental cross sections can be obtained using either the information from the monitors or from the beam current integrator plus the target thickness to normalize them. The values obtained with these two different methods agree within 2%.

At the higher energies, 100*A*, 130*A* and 155*A* MeV, there were discrepancies between the experimental elastic cross section and the Rutherford one, due to the fact that the grazing angle was getting close to that of the monitors. Therefore, the beam current integrator was used to get the cross sections. The check at the lowest energy gives us some confidence in this procedure. The relative solid angles were checked using a ^{228}Th α source.

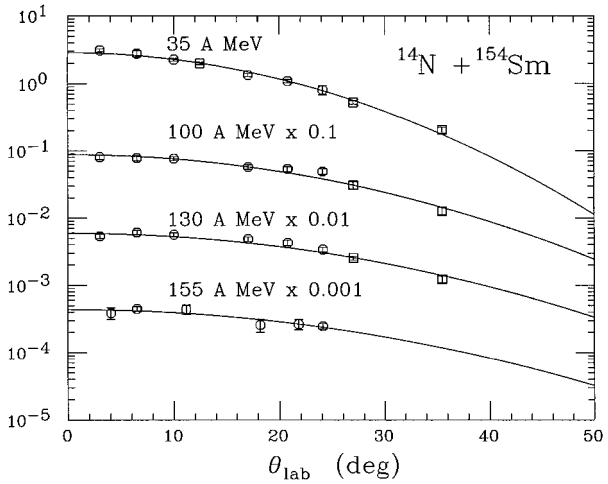

FIG. 1. Angular distributions of evaporation residues for the ^{14}N+^{154}Sm system at 35*A*, 100*A*, 130*A*, and 155*A* MeV. The open circles represent data taken with the Si detectors, and the open squares are from the ion chamber detectors. The full curve is a fit used to obtain the angle-integrated cross section.

Typical ER angular distributions are shown in Fig. 1. The parameters of a Gaussian were adjusted to match the ER differential cross sections with a least squares minimization procedure. The optimum fit was integrated over angle to get the total ER cross sections, which are listed in Table I.

The total fission cross section at a given energy was obtained by transforming the angular distributions from the laboratory frame to the center of mass frame. The transformation was made assuming that the target captures a fraction of the projectile (to simulate pre-equilibrium particle emission) and then undergoes symmetric fission. The effective projectile that was assumed to be captured had the same velocity as the projectile and was obtained by requiring that the resulting transformed angular distribution be symmetric in the c.m. system. Each angular distribution was fitted with a Legendre polynomial of even terms up to order 4 and integrated. A typical FF angular distribution is shown in Fig. 2, and the FF cross sections are listed in Table I. The fusion cross section, defined as $\sigma_{\rm ER}+\sigma_{\rm FF}$, is listed in Table I. The ratio of the masses of the effective projectile captured and that of the projectile gives us an estimate of the average linear momentum transfered (LMT) and is listed in Table II.

IV. FISSION FRAGMENT COINCIDENCE DISTRIBUTIONS

The fission fragment folding angles, ($\theta_f=\theta^{\rm lab}_{\rm FF_1}+\theta^{\rm lab}_{\rm FF_2}$) were analyzed for the reactions 35*A* and 100*A* MeV ^{14}N on ^{181}Ta. We are also presenting results of 25*A* MeV ^{16}O on the same target. Ion chamber detectors placed at 45°, 57°, and 72° were used as triggers, leading to the coincident fragment being detected in the Miniball.

A Monte Carlo simulation was developed to reproduce the experimental folding angle distributions and extract the mean LMT $\langle v\rangle/\langle v_0\rangle$ to the fissioning nucleus, v is the emitter

TABLE I. ER, FF, and total fusion cross sections determined in this work. Also tabulated are the critical ℓ values for evaporation residue formation (ℓ_c^{er}) and for fusion (ℓ_c^{fus})deduced by the sharp cutoff model. The mean ℓ, $\langle\ell\rangle$, for ER and FF is also calculated using the same model. The last column gives the maximum angular momentum left in the composite system. The FF cross sections from the ^{197}Au target have some deeply inelastic fission contamination and the asterisks were used to indicate the quantities affected by this fact.

System		σ_{ER}	σ_{FF}	σ_{FUS}	ℓ_c^{er}	$\langle\ell\rangle_{ER}$	ℓ_c^{fus}	$\langle\ell\rangle_{FF}$	Jm
35*A* MeV	^{14}N+^{154}Sm	1200±180	70±10	1270±180	104±7	69	107±7	106	92
	^{14}N+^{159}Tb	1040±160	160±20	1200±160	97±7	65	105±7	102	90
	^{14}N+^{197}Au	300±40	1420±190*	1720±200*	53±3	35	127±7*	96*	72*
100*A* MeV	^{14}N+^{154}Sm	570±70	60±10	630±70	121±7	81	129±7	126	55
	^{14}N+^{159}Tb	610±100	110±20	720±100	126±11	84	137±10	133	59
	^{14}N+^{197}Au	470±90	480±40*	950±100*	112±10	75	159±8*	138*	46*
130*A* MeV	^{14}N+^{154}Sm	470±90	70±10	540±90	125±12	84	135±11	129	58
	^{14}N+^{197}Au	330±70	320±30*	650±80*	107±9	71	151±8*	131*	44*
155*A* MeV	^{14}N+^{154}Sm	380±120	80±30	460±120	123±19	82	136±18	130	59
	^{14}N+^{197}Au	320±100	270±70*	590±120*	115±17	77	157±16*	138*	45*

velocity for a given fraction of LMT and v_0 is the velocity of the composite system resulting from fusion with full LMT. This fraction $\langle v\rangle/\langle v_0\rangle$ is determined not only by the mass of the pre-equilibrium particle but also by the momentum that the particle can carry away as one can see in the following description. First the projectile-target system, the beam energy, and the detector geometry were described by the input. Then, event by event, we parametrize the incomplete fusion by prompt particle emission using a Poisson distribution. Since the proportion of different prompt particles (p,d,t,α) does not change much with bombarding energy, the only parameter that was varied was the average multiplicity. The distribution of momentum carried away by each pre-equilibrium particle is described by a Gaussian centered about $(3/4)v_p$ and a standard deviation $\sigma=(1/4)v_p$, where v_p is the projectile velocity. This choice is somewhat arbitrary, but the LMT is mainly sensitive to the combination of the velocity and the multiplicity of the emitting particles.

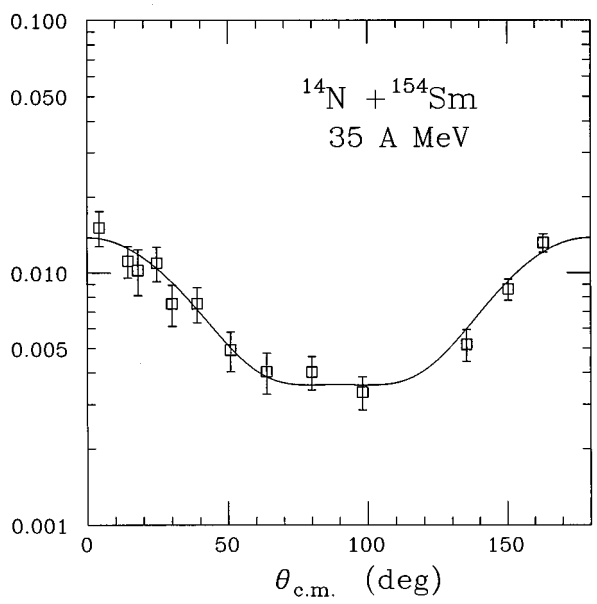

FIG. 2. Fission fragments angular distribution for the ^{14}N+^{154}Sm system at 35*A* MeV. The velocity of the center of mass was obtained by requiring fore-aft symmetry in the c.m. frame and corresponds to capture of 12/14 of the projectile. The full curve is a fit used to obtain the angle integrated cross section.

The mass and momentum transferred to the target characterizes the fissioning composite system via complete fusion. A Gaussian was used to describe the symmetric mass split of the excited system with a $\sigma=(1/4)A_{fus}$, where A_{fus} refers the mass of the fissioning system. The total kinetic energy of the FF was calculated using Viola systematics [13]. Finally, the FF angular distribution was weighted by $1/\sin\theta_{c.m.}$, and their energy E_{lab}^{FF} and directions θ_{lab} and ϕ_{lab} were checked for geometry and energy threshold requirements. The experimental folding angle distributions were then compared to the calculated ones based on a minimization approach.

The results of these fits as well as the $\langle v\rangle/\langle v_0\rangle$ extracted are shown in Fig. 3 for a trigger angle of ($\theta_{IC}=57.5°$). The experimental folding angles θ_f^{exp} are represented by circle symbols. The statistical and systematic errors associated with them are also reported here. The dashed histogram represents the minimized fit. As expected, $\langle v\rangle/\langle v_0\rangle$ decreases with increasing bombarding energy. This trend was observed for all trigger angles.

Finally, in Fig. 4 we summarize our results by presenting the variation of $\langle v\rangle/\langle v_0\rangle$ as a function of the relative velocity of the system at the contact point. These points were obtained by averaging over 3 trigger angles (45°, 57°, and 72°) and the error associated with them were estimated from the angular resolution.

V. DISCUSSION

There are not many published results for fusion cross sections in this energy and mass range. There is one study for ^{14}N+^{154}Sm at 19*A* MeV and 35*A* MeV [14] the latter of which can be directly compared with our results. They measured ER differential cross sections which are about half of our values and have a somewhat different shape. Also, their integrated ER cross section at 19*A* MeV (around 700 mb) seems to be smaller than what one would expect on the basis of other measurements in that mass and energy range [15]. The system ^{20}Ne(30*A* MeV)+^{165}Ho was studied in Ref. [16], where they report ER and FF cross sections of 1550 mb and 805 mb, values close to the present work.

TABLE II. Nucleus captured at beam velocity which gives a momentum transfer consistent with the fore-aft asymmetry of the laboratory fission fragment angular distributions and the corresponding percentage of linear momentum transfer. The FF cross sections from the ^{197}Au target have some deeply inelastic fission contamination and the asterisks were used to indicate the quantities affected by this fact.

System		% LMT
35*A* MeV	^{14}N+^{154}Sm	86±7
	^{14}N+^{159}Tb	86±7
	^{14}N+^{197}Au	57±14*
100*A* MeV	^{14}N+^{154}Sm	43±7
	^{14}N+^{159}Tb	43±7
	^{14}N+^{197}Au	29±14*
130*A* MeV	^{14}N+^{154}Sm	43±14
	^{14}N+^{197}Au	29±14*
155*A* MeV	^{14}N+^{154}Sm	43±14
	^{14}N+^{197}Au	29±14*

The fission cross section for ^{14}N(35*A* MeV)+^{197}Au (1400 mb) is somewhat large when compared to the other systems. It is however comparable to the values of 900 and 400 mb for the slightly less fissionable composite system formed in 35*A* MeV and 85*A* MeV ^{12}C+^{197}Au reported in [17]. We believe that this enhancement is due to a contribution of fission following deeply inelastic scattering. The fissionability of the ^{197}Au target is much larger than that of the other targets. This interpretation is supported by the anomalously small values of the LMT required to symmetrize the fission fragment angular distribution (Table II). In a study of the system ^{20}Ne(30*A* MeV)+^{197}Au [18], the fusion-fission cross section, where the contribution from low-momentum-transfer fission was removed, was measured to be 1600 mb.

The fission cross sections for different targets and projectiles at 20*A* MeV can be found in [19]. They are in good agreement with an extrapolation of our results at the lowest energies.

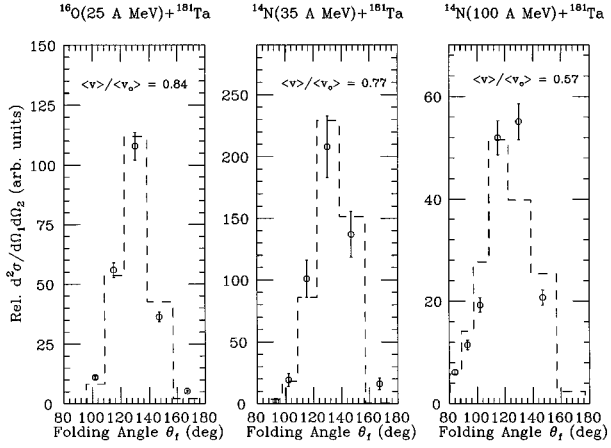

FIG. 3. Examples of experimental fission fragment folding angle distributions for 25*A* MeV ^{16}O+^{181}Ta, 35*A* MeV ^{14}N+^{181}Ta and 100*A* MeV ^{14}N+^{181}Ta. One of the fission fragments was detected with the ion chamber at 57.5°. The dashed curves represent the best fits.

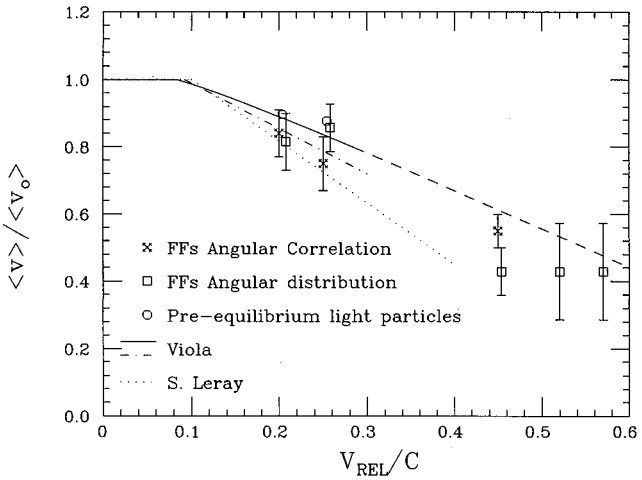

FIG. 4. Ratio of composite system velocity to velocity for complete fusion as a function of the relative velocity at contact. The crosses represent data from fission fragment folding angle distributions and the squares represent data from symmetrizing fission fragment angular distribution. The circles are deduced from the linear momentum carried away by light pre-equilibrium particles. The curves are from the systematics of Viola and Leray as discussed in the text.

The critical ℓ values for fusion, $\ell_c^{\rm fus}$, determined from the sum of the ER and FF cross sections, increase with bombarding energy and considerably exceed the ℓ value for which the fission barrier goes to zero ($\ell_{Bf=0}\sim 80$). This might be at first troubling but we must remember that the ℓ value here refers to the angular momentum of the incoming partial wave, not the angular momentum deposited in the composite nucleus. Pre-equilibrium particle emission increases with increasing bombarding energy and is responsible for loss of both linear momentum and angular momentum. We can make use of our results on LMT to estimate the mean and maximum values of angular momentum left in the composite system after pre-equilibrium particle emission. If the impact parameter (over the range of impact parameters leading to fusion) dependence of pre-equilibrium particle emission is neglected, the maximum angular momentum J_m resulting from $\ell_c^{\rm fus}$ can be obtained simply from the average momentum transfer by assuming that the fraction of angular momentum retained by the composite system is the same as the fraction of linear momentum retained. These values are indicated in Table I. It can be seen that they are generally comparable to or less than the angular momentum for which the fission barrier vanishes ($\ell_{Bf=0}\sim 80$).

One can qualitatively account for the bombarding energy dependence of the fusion cross section by incorporating this incomplete fusion picture into a model proposed by Bass [20]. In this model, the criterion for fusion is whether the attractive nuclear force exceeds the repulsive Coulomb and centrifugal forces at the contact point after kinetic energy and angular momentum dissipation by friction. Comparison between calculations and experimental data is shown in Fig. 5 for ^{14}N+^{154}Sm and ^{14}N+^{197}Au, which are the only systems for which the fusion cross section was measured in the entire energy range. The dashed curve in Fig. 5 is the calculated fusion cross section as a function of the center of mass energy using as the ''projectile'' that fraction of the true pro-

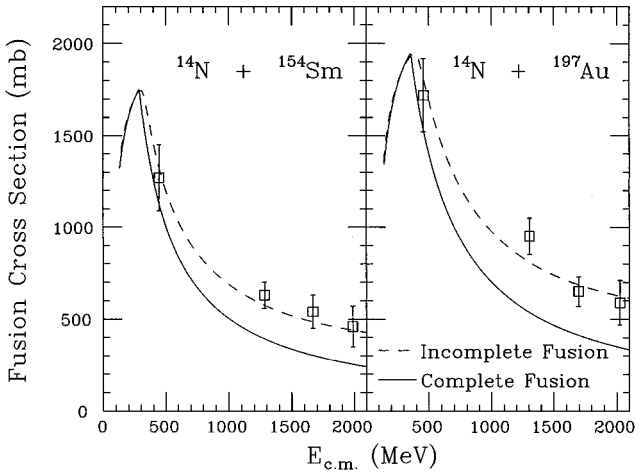

FIG. 5. Bombarding energy dependence of fusion cross section for the ^{14}N+^{154}Sm and ^{14}N+^{197}Au systems. The open squares represent our experimental data. The full curve is a Bass model calculation assuming complete fusion of the projectile. The dashed curve assumes capture of that fraction of the projectile required to reproduce the linear momentum transfer given by the Viola systematics.

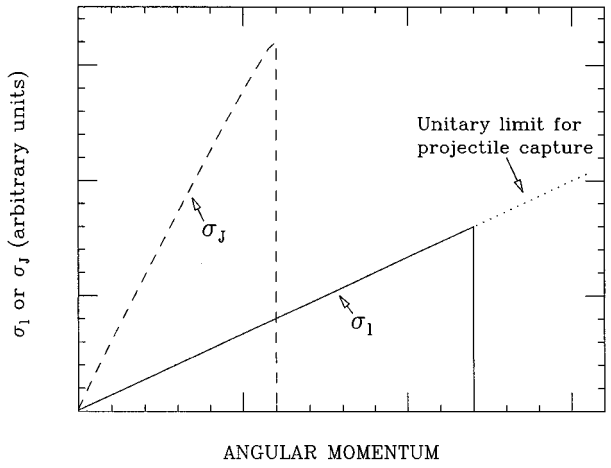

FIG. 6. Illustration of initial projectile partial wave cross section σ_ℓ and composite system partial spin cross section σ_J when only half of the projectile with beam velocity is captured.

jectile mass required to give a LMT consistent with the Viola systematics [6] for LMT. There are two adjustable parameters, one of which is the fraction of the initial orbital angular momentum f not transfered into internal rotation by friction. To reproduce the overall magnitude of the cross section, we have taken $f=0.55$ for ^{154}Sm and $f=0.5$ for ^{197}Au, values which are intermediate between the rolling (5/7=0.7) and the sticking (0.3) limits. A similar calculation assuming complete fusion is indicated by the full curve. The other parameter is the diffuseness of the nuclear potential and our data are not sensitive to reasonable variations on it so we set it equal to 1 fm.

The above picture, if it is assumed that incomplete fusion is only occurring for the largest partial waves, is not correct as in fact pre-equilibrium particle emission occurs for all partial waves and the angular momentum J deposited in the composite system will in general be less than ℓ for each partial wave. The expected final result is sketched in Fig. 6. The dashed curve gives the expected final J distribution for a partial wave distribution given by the full line. One sees that the partial cross sections for making a composite system of angular momentum J after pre-equilibrium particle emission exceed the unitary limit in the absence of pre-equilibrium particle emission, an effect that was anticipated some time ago [21].

It is important to point out that studies using the folding angle technique on highly fissionable targets [22–24] might suggest that the fusion cross section would vanish at energies higher than 50 MeV per nucleon. The results reported here seem to disagree with these previous findings, however one must remember that for highly fissionable targets like U or Th, most of the fission events are produced after inelastic collisions where little linear momentum is transfered and the folding angle takes a value close to 180°. As a result, the folding angle distribution becomes dominated by the presence of the low-momentum transfer peak and fission events from fusion reactions are difficult to distinguish. Therefore the disappearance of fusion should not be tested using the folding angle technique with highly fissionable targets.

We turn now to a discussion of the LMT values. One should keep in mind that because of the low fissionability of Sm, Tb, and Ta, we do not expect them to fission following deeply inelastic scattering. Au however is sufficiently fissionable that one can expect some contribution for fission following deeply inelastic scattering, as well as following fusion. This expectation is supported by the large fission cross section we measured and the small value of LMT required to symmetrize the fission fragment angular distribution for this target.

The bombarding energy dependence of the LMT in fusion reactions, expressed as the ratio of the observed composite system velocity to that expected from complete fusion, is illustrated in Fig. 4, where Au is excluded. A good agreement is seen between the LMT values coming from the symmetrization of the FF angular distribution and the folding angle technique.

Leray has suggested [25] that the LMT scales as the relative velocity at contact, and this is the parameter we have used as the abscissa in Fig. 4. The dotted line represents the fit Leray obtained to a broad range of data. For highly fissionable targets such as Th or U it is more appropriate to compare with the most probable momentum transfer, reflecting fusionlike processes, rather than the average momentum transfer which includes contributions from very peripheral, quasi- and deeply-inelastic scattering. The dashed dot curve in Fig. 4 is the trend exhibited by ^{12}C and ^{14}N fission of U as summarized by Viola [26]. Our results are in good agreement with these. They are also in reasonable agreement with the original systematics of Viola *et al.* [6] in the range where it originally extended, noted by a full line. A dashed line indicates an extrapolation to higher values of E/A and it overestimates the experimental values, something that is also observed by Fahli *et al.* [9]. The LMT value for Au can be compared with the average LMT measured for highly fissionable targets reported by Viola in [26] and a good agreement was observed.

One can estimate the LMT separately for the parts of the fusion cross section leading to fission and that leading to

evaporation residues by making use of the information on pre-equilibrium particle emission obtained as part of this experiment. The pre-equilibrium particle data will be presented elsewhere, but we have made a preliminary estimate of the linear momentum lost to pre-equilibrium particle emission using the source velocity and multiplicities deduced from p,d,t, and α energy and angular distributions. A small correction was made for neutrons which were not detected. These values are in reasonable agreement with the values obtained from the fission fragment-fission fragment folding angle distributions and for symmetrizing the fission fragment anisotropy data. The TAMU group [14] also measured the fraction of LMT for $^{14}\mathrm{N}+^{154}\mathrm{Sm}$ at 35A MeV by measuring the ER velocities and reported $0.61 +- 0.07$, a value smaller than ours.

In summary, a consistent picture has emerged where as the bombarding energy increases, fusionlike processes can occur for an increasing number of partial waves with ℓ_c^{fus} well beyond the angular momentum value for which the fission barrier of the composite system goes to zero. This occurs because the angular momentum finally appearing in the composite system is reduced by pre-equilibrium particle emission to values which the system can accommodate without instantly fissioning. The relatively large fusion cross sections even at bombarding energies exceeding 100A MeV make possible a number of interesting experiments using fusion products as tags for central collisions.

ACKNOWLEDGMENT

This work was supported in part by the U.S. Department of Energy and the National Science Foundation.

[1] M.B. Tsang, G.F. Bertsch, W.G. Lynch, and M. Tohyama, Phys. Rev. C **40**, 1685 (1989).
[2] M.B. Tsang, Y.D. Kim,, N. Carlin, Z. Chen, R. Fox, C.K. Gelbke, W.G. Gong, W.G. Lynch, T. Murakami, T.K. Nayak, R.M. Ronningen, H.M. Xu, and F. Zhu, Phys. Lett. B **220**, 492 (1989).
[3] L. Phair, D.R. Bowman, C.K. Gelbke, W.G. Gong, Y.D. Kim, M.A. Lisa, W.G. Lynch, G.F. Peaslee, R.T. de Souza, M.B. Tsang, and F. Zhu, Nucl. Phys. **A548**, 489 (1992).
[4] D. Prindle, R. Vandenbosch, S. Kailas, A. Charlop, and C. Hyde-Wright, Phys. Rev. C **48**, 291 (1993).
[5] M. B. Tsang (private communication).
[6] V.E. Viola, Jr., B.B. Back, K.L. Wolf, T.C. Awes, C.K. Gelbke, and H. Breuer, Phys. Rev. C **26**, 178 (1982).
[7] M.B. Tsang, D.R. Klesch, C.B. Chitwood, D.J. Fields, C.K. Gelbke, W.G. Lynch, H. Utsunomiya, K. Kwiatkowski, V.E. Viola, Jr., and M. Fatyga, Phys. Lett. **134B**, 169 (1984).
[8] M. Fatyga, K. Kwiatkowski, V.E. Viola, C.B. Chitwood, D.J. Fields, C.K. Gelbke, W.G. Lynch, J. Pochodzalla, and M.B. Tsang, Phys. Rev. Lett. **55**, 1376 (1985).
[9] A. Fahli, J.P. Coffin, G. Gillaume, B. Heusch, F. Jundt, F. Rami, P. Wagner, P. Fintz, A.J. Cole, S. Kox, and Y. Schutz, Phys. Rev. C **34**, 161 (1986).
[10] R.T. DeSouza, N. Carlin, Y.D. Kim, J. Ottarson, L. Phair, D.R. Bowman, C.K. Gelbke, W.G. Gong, W.G. Lynch, R.A. Pelak, T. Peterson, G. Poggi, M.B. Tsang, and H.M. Xu, Nucl. Instum. Methods A **295**, 109 (1990).
[11] Y.D. Kim, Ph.D. thesis, Michigan State University, 1991 (unpublished).
[12] M.B. Tsang, R.T. de Souza, Y.D. Kim, D.R. Bowman, N. Carlin, C.K. Gelbke, W.G. Gong, W.G. Lynch, L. Phair, and F. Zhu, Phys. Rev. C **44**, 2065 (1991).
[13] V.E. Viola, K. Kwiatowski, and M. Walker, Phys. Rev. C **31**, 1550 (1985).
[14] K. Hagel, D. Fabris, P. Gonthier, H. Ho, Y. Lou, Z. Majka, G. Mouchaty, M.N. Namboodiri, J.B. Natowitz, G. Nebbia, R.P. Schmitt, G. Viesti, R. Wada, and B. Wilkins, Nucl. Phys. **A486**, 429 (1988).
[15] R. Kossakowski, S. Andre, J. Genevey, A. Gizon, V. Barci, D. Barneoud, A. Charvet, C. Foin, and J. Salicio, Phys. Rev. C **33**, 1514 (1986).
[16] D. Hilscher, H. Rossner, A. Gamp, U. Jahnke, B. Cheynis, B. Chambon, D. Drain, C. Pastor, A. Giorni, C. Morand, A. Dauchy, P. Stassi, and G. Petitt, Phys. Rev. C **36**, 208 (1987).
[17] K. Aleklett, M. Johansson, L. Sihver, W. Loveland, H. Groenig, P.L McGaughey, and G.T. Seaborg, Nucl. Phys. **A499**, 591 (1989).
[18] G. La Rana, G. Nebbia, C. Ngo, X.S. Chen, S. Leray, P. Lhenoret, R. Lucas, C. Mazur, M. Ribrag, C. Cerruti, S. Chiodelli, A. Demeyer, D. Guinet, J.L. Charvet, M. Morjean, A. Peghaire, Y. Pranal, L. Sinopoli, and J. Uzureau, Nucl. Phys. **A407**, 233 (1983).
[19] A. Gavron, J. Boissevain, H.C. Britt, K. Eskola, M.M. Fowler, H. Ohm, J.B. Wilhelmy, T.C. Awes, R.L. Ferguson, F.E. Obenshain, F. Plasil, and G.R. Young, Phys. Rev. C **30**, 1550 (1984).
[20] R. Bass, Nucl. Phys. **A231**, 45 (1974).
[21] R. Vandenbosch, in *Heavy Ion Fusion Reactions*, Proceedings of the Tsukuba International Symposium, 1984, edited by K. Furuno and T. Kishimoto (World Scientific, Singapore, 1984), p. 355.
[22] E.C. Pollacco, M. Conjeaud, S. Harar, C. Volant, Y. Cassagnou, R. Dayras, R. Legrain, M.S. Nguyen, H. Oeschler, and F. Saint-Laurent, Phys. Lett. **146B**, 29 (1984).
[23] D. Jacquet, E. Duek, J.M. Alexander, B. Borderie, J. Galin, D. Gardes, D. Guerreau, M. Lefort, F. Monnet, M.F. Rivet, and X. Tarrago, Phys. Rev. Lett. **53**, 2226 (1984).
[24] M. Conjeaud, S. Harar, M. Mostefai, E.C. Pollacco, C. Volant, Y. Cassagnou, R. Dayras, R. Legrain, H. Oeschler, and F. Saint-Laurent, Phys. Lett. **159B**, 244 (1985).
[25] S. Leray, J. Phys. (Paris) Colloq. **47**, C4-275 (1986).
[26] V.E. Viola, Nucl. Phys. **A502**, 531c (1989).